DELAMINATION FRACTURE TOUGHNESS

OF A UNIDIRECTIONAL COMPOSITE

A Thesis

by

Daniel Frank Devitt

Approved as to style and content by:
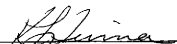
_(W.L. Bradley, Chairman)_
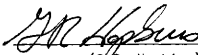
_(R.A. Schapery)_
(Member)

_(K.L. Jerina )_
(Member)

_(Y. Weitsman)_
(Member)

_(G.R. Hopkins)_
(Head of Department)

August 1979

ABSTRACT

Delamination Fracture Toughness of a Unidirectional

Composite. (August 1979)

Daniel Frank Devitt, B.S. A. & A.E., Purdue University;

Chairman of Advisory Committee: Dr. W. L. Bradley

An analytical technique for reducing experimental data is
developed for a unidirectional composite in order to determine the
delamination fracture toughness for the crack opening mode. A
unique characteristic of this data reduction technique is that the
crack opening mode is isolated from the other fracture processes.
Isolation of this fracture mode allows for the direct determination
of the critical energy release rate ($G_c$) and the critical stress
intensity factor ($K_{IC}$).

The values for the critical energy release rate and the critical
stress intensity factor were calculated using linear elastic fracture
mechinics coupled with nonlinear beam theory. The critical energy
release rate is found from utilizing linear elastic fracture mechanics
as it is related to the release of the stored strain energy in the
system. Nonlinear beam theory is required to calculate the strain
energy in the system, since large deflections and rotations are
produced experimentally and are not accounted for in linear beam
theory.

## ACKNOWLEDGEMENTS

The author would like to express his gratitude to Vought Corporation, Texas A&M University, and the Air Force Office of Scientific Research for allowing him to have the opportunity to participate in the Advanced Composite Master's Program. Appreciation is extended to the faculty and staff associated with this program for their assistance in technical, as well as administrative problems.

To my chairman, Dr. W.L. Bradley, many thanks for the cooperation and patience which he extended during the preparation of this research project. Additional graditude is offered to members of my research committee, Dr. R.A. Schapery, Dr. Y. Weitsman, and Dr. K.L. Jerina for their useful comments and suggestions.

I would also like to express my deepest gratitude to Mary. For, without her unending support and encouragement throughout the duration of the program, I would never have been able to clear the major obstacles which were encountered.

I would like to express my fondest appreciation to my grandparents, Dr. and Mrs. Raymond S. Fisher, for their assistance in my undergraduate years which made this all possible.

## TABLE OF CONTENTS

LIST OF TABLES

TABLE

## LIST OF FIGURES

FIGURE

## INTRODUCTION

This research effort was directed toward the development of a method for determining the delamination fracture toughness in the crack opening mode for a unidirectional composite. The plane strain fracture toughness of a material, may be characterized by the critical stress intensity factor ($K_{IC}$) or the critical energy release rate ($G_c$). The approach to determine these material properties for high-strength metals using linear elastic fracture mechanics is well established [1]. This approach, however, does not readily apply to composite materials. As the requirements for light-weight, high-strength materials have increased, so has the use of fiber-reinforced composites. Subsequently, the need has arisen to develop a similar analytical and experimental approach to characterize the fracture behavior of composite materials.

The fracture toughness behavior of metallic materials can normally be described by a single parameter such as $K_{IC}$. However, fracture in a composite is much more complicated since there are three main sources of energy dissipation during the fracture process in composites: (1) fiber breakage, (2) matrix failure, and (3) fiber-matrix decohesion. The latter two processes dominate the delamination fracture phenomenon considered in this effort.

A survey of the current literature did not reveal an acceptable procedure for determining independently the critical stress intensity

---

This thesis uses the format of the Journal of Composite Materials.

for mode I delamination fracture. Previous investigations [2 - 4] have been carried out for the delamination phenomenon utilizing the specimen depicted in Figure 1. Reduction of the data for this particular specimen requires a knowledge of the ratio of the stress intensity factors for the opening (I) and the shearing (II) modes [5]. This is due to the presence of interlaminar shear. The presence of both of these modes complicates the analysis required to interpret and reduce the data.

However, the crack opening mode can be isolated using the specimen shown in Figure 2. The stress intensity factor for this double cantilever beam is given [6] as:

$$K_I = \frac{CPL}{\sqrt{2BI}}$$

or                                                                          (1)

$$K_I = \frac{3CE\Delta}{L^2}\sqrt{\frac{I}{2B}}$$

where        $K_I$ = stress intensity factor for the crack opening mode

             C = plane stress/strain correction factor

             P = applied load

             L = effective beam length

             B = beam width

             I = moment of inertia

             E = modulus of elasticity

             $\Delta$ = load displacement

The relationship presented in Equation (1) is not applicable in the calculation of $K_I$ when large deflections and rotations are present in the double cantilever beam due to non-linear effects ignored in
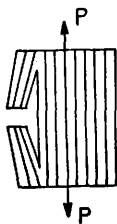
Figure 1. Wang/Mandell Specimen
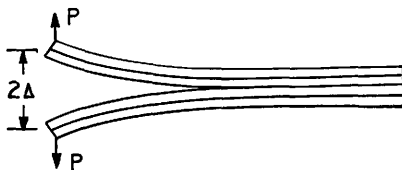


Figure 2. Double cantilever beam specimen

the derivation of Equation (1).

Using non-linear beam theory, the critical energy release rate has been calculated as a function of $\Delta/L$, which has been determined experimentally. The main body of this thesis developed this data reduction technique. Experimental verification has been done using three different beam thicknesses of the double cantilever beam specimen of Figure 2. Upon determining the critical energy release rate $(G_c)$ the critical stress intensity factor $(K_{IC})$ was readily found [5] to be:

$$K_{IC} = (\hat{E} G_c)^{1/2} \tag{2}$$

where      $\hat{E}$ = effective modulus (The effective modulus $\hat{E}$ is approximately equal to one half the transverse modulus $(E_{22})$ for an orthotropic material [7]).

## ANALYTICAL PROCEDURE

The analytical procedure draws on linear elastic fracture mechanics theory to determine the realtionship between the critical energy release rate and the strain energy stored in the beam. Determination of the stored strain energy is accomplished using non-linear beam theory. The particular derivations are shown in the remainder of this section.

### Energy Release Rate (G)

The energy release rate is that amount of energy that is released during the fracture process in the creation of one unit of surface area. This release rate is related to the change in the stored strain energy and the external work done on the system during crack propagation. For a given material the energy release rate per unit of crack extension is characterized as a material parameter ($G_c$), the critical energy release rate, at the initiation of crack extension.

$$G = \frac{dU}{Bda} = \frac{Pd\Delta}{Bda} - \frac{dW}{Bda} \qquad (3)$$

G = energy release rate

U = total elastic energy of the system

B = specimen width

a = crack length

P = external load

Δ = load displacement

W = total strain energy

Hertzberg has noted that this relationship is independent of the test conditions used "...(e.g., fixed grip, constant load, combinations of load change and displacement, and machine stiffness)." [5]. The implications of this are that one can run any type test and, with proper analysis, determine the value of $G_c$. A convenient form of Equation (3) can be derived by holding the displacement constant.

$$G = - \left( \frac{\delta W}{B \delta a} \right) \Delta = \text{constant} \tag{4}$$

To successfully evaluate the critical energy release rate the strain energy must be written as a function of the crack length. Non-linear beam theory will be used to evaluate the strain energy to be used in Equation (4).

## Strain Energy (W)

The strain energy in a cantilever beam under a concentrated end load is found from elementry beam theory to be,

$$W = \frac{1}{2} \int_0^L \frac{M^2}{EI} \, ds \tag{5}$$

where
    W = strain energy

    L = beam length

    M = moment

    E = longitudinal bending modulus

    EI = flexural rigidity of the beam

The assumptions of linear beam theory breakdown when large deflections and rotations are present in the system. As a result of the low flexural rigidity of a composite specimen fabricated from

a thin laminate, large deflections and rotations are present during the test, and need to be accounted for in the analysis. Such a correction to linear beam theory has been done by Bisshopp and Drucker [8] where they included the effect of the square of the first derivative in the curvature formula and the effect of beam shortening of the moment arm during delfection.

The nomenclature and geometric relationships used by Bisshopp and Drucker are shown in Figure 3. The principal equations in Bisshopp and Drucker's analysis are:

$$\left(\frac{PL^2}{EI}\right)^{1/2} = \frac{\sqrt{2}}{2} \int_0^{\phi_0} (\sin\phi_0 - \sin\phi) \, d\phi \qquad (6)$$

$$\Delta = \left(\frac{EI}{2P}\right)^{1/2} \int_0^{\phi_0} \frac{\sin\phi}{(\sin\phi_0 - \sin\phi)^{1/2}} \, d\phi \qquad (7)$$

where    P = applied load

L = undeformed beam length

EI = flexural rigidity

$\phi_0$ = angle of slope at the loaded end

$\Delta$ = load displacement

$\phi$ = slope of beam.

After determining the appropriate change of variables and transformations Bisshopp and Drucker were able to rearrange Equation (6) and Equation (7) into canonical elliptic form as shown below:

$$\left(\frac{PL^2}{EI}\right)^{1/2} = F(k) - F(k, \phi) \qquad (8)$$
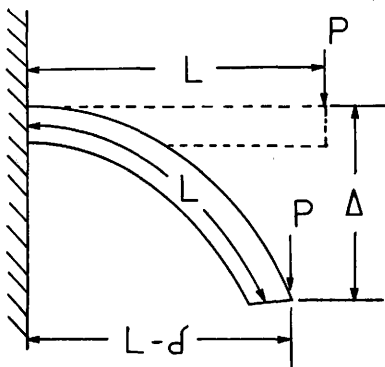
Figure 3. Cantilever beam nomenclature

$$\frac{\Delta}{L} = 1 - 2 \left( \frac{E(k) - E(k, \phi)}{F(k) - F(k, \phi)} \right) \tag{9}$$

where    $F(k)$ = complete elliptic integral of the first kind

   $F(k,\phi)$ = incomplete elliptic integral of the first kind

   $E(k)$ = complete elliptic integral of the second kind

   $E(k,\phi)$ = incomplete elliptic integral of the second kind

   $k, \phi$ = elliptic parameters [9]

A table listing the pertinent elliptic integral data is presented in
Appendix A. Since Bisshopp and Drucker's results are univalued
functions of the same elliptic parameters, the results can be shown to
be functions of each other, see Figure 4. This result will be used
later in the data reduction section. The data pairs used to generate
Figure 4 are tabulated in Appendix B.

Having an acceptable means of correcting linear beam theory under
the conditions of large deflections and rotations, one can now evaluate
the strain energy. Following Bisshopp and Drucker's substitution and
reduction procedure, Equation (5) can be written in terms of the
elliptic functions tabulated in Appendix A as follows:

$$\frac{WL}{EI} = (F(k) - F(k, \phi))^2 \left( \frac{E(k) - E(k, \phi)}{F(k) - F(k, \phi)} + 2(k^2 - 1) \right) \tag{10}$$

A detailed derivation of Equation (10) is presented in Appendix C.
Thus, determination of the strain energy now enables us to evaluate
the critical energy release rate using Equation (4) and the appropriate
test data.
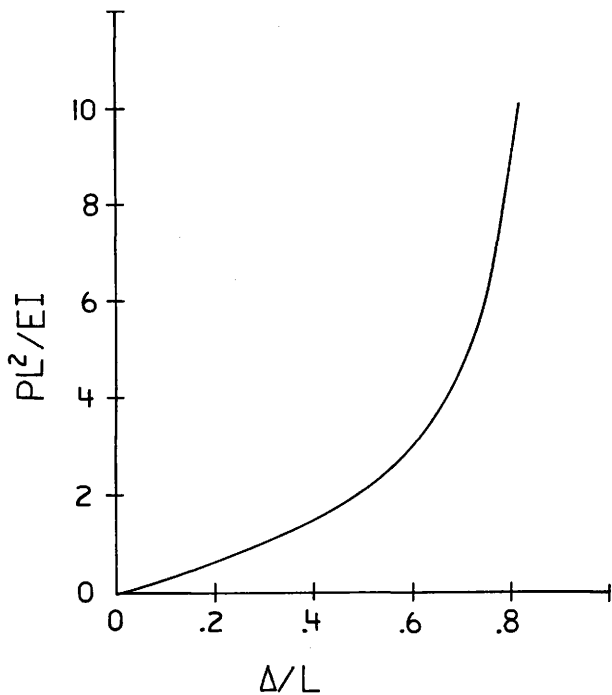
Figure 4. (PL$^2$/EI) vs. ($\Delta$/L)

## Analytical Data Reduction

Incorporating the strain energy into Equation (4) requires some slight data manipulation for the particular test involved. From the data in Appendix B one can produce the non-dimensionalized strain energy as a function of $\Delta/L$, see Figure 5. Recalling Equation (4) it is noted that strain energy must be differentiated with respect to crack length while the load displacement is held constant. However, in our experiment a change in crack length directly results in a change in the effective beam length. Furthermore, the total strain energy in the system is obtained by considering both sections in the double canti-lever beam. Due to symmetry, the resulting critical energy release rate can be calculated from the strain energy in one beam as follows:

$$G_c = 2 \left( \frac{\delta W}{B \delta L} \right) \; \Delta = \text{constant} \tag{11}$$

In order to evaluate $G_c$ consider the following relationships. Since

$$\frac{WL}{EI} = f(\Delta/L) \qquad \text{(see Figure 5)}$$

and

$$W = \frac{EI}{L} \; f(\Delta/L)$$

then

$$\left( \frac{\delta W}{\delta L} \right)_{\Delta \; = \; \text{constant}} = \frac{-EI}{L^2} \left( f(\Delta/L) + (\Delta/L) \; \frac{\delta f(\Delta/L)}{\delta L} \right) \; .$$

It is easily shown that

$$(\Delta/L) \; \frac{\delta f(\Delta/L)}{\delta L} = \left( \frac{WL}{EI} \right) \left( S \right)$$
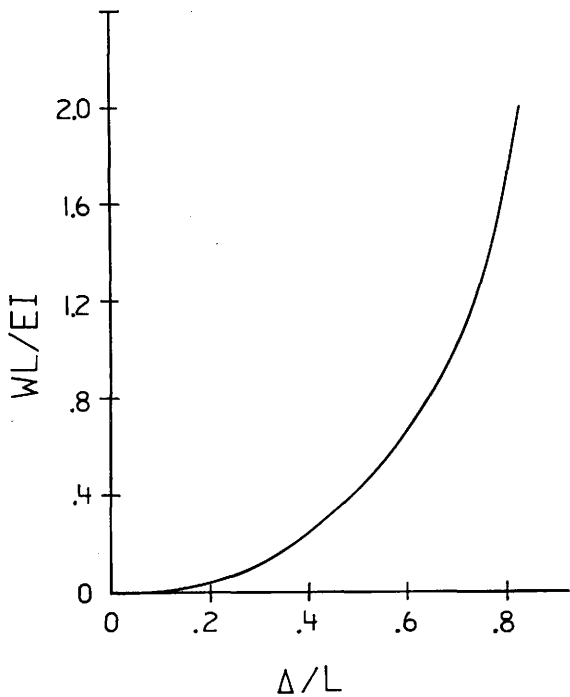
Figure 5. (WL/EI) vs. (Δ/L)

where

$$S = \text{local slope of the } \ln \frac{WL}{EI} \text{ vs. } \ln \frac{\Delta}{L} \text{ graph.}$$

Therefore,

$$G_c = -\left(\frac{\delta W}{B\delta L}\right)_{\Delta\,=\,\text{constant}} = \frac{EI}{BL^2}\left(\frac{WL}{EI}\right)\left(1 + S\right) \tag{12}$$

A graphical representation of S is constructed in Figure 6. A re-arrangement of Equation (12) yields the non-linear form of the critical energy release rate:

$$\frac{G_c BL^2}{EI} = \frac{WL}{EI}\,(1 + S) \tag{13}$$

Since both WL/EI and S in Equation (13) are functions of $\Delta/L$, $G_c BL^2/EI$ is an implicit function of $\Delta/L$. Using Equation (13) in conjunction with Figures 5 and 6, $G_c BL^2/EI$ as a function of $\Delta/L$ has been evaluated and presented graphically in Figure 7.

The derived analytical data reduction technique, resulting in the relationship displayed in Figure 7, will allow the desired material properties to be determined for experimentally determined values of $\Delta/L$. In the next section an experimental procedure compatible with this analysis, to measure $\Delta/L$, will be described.
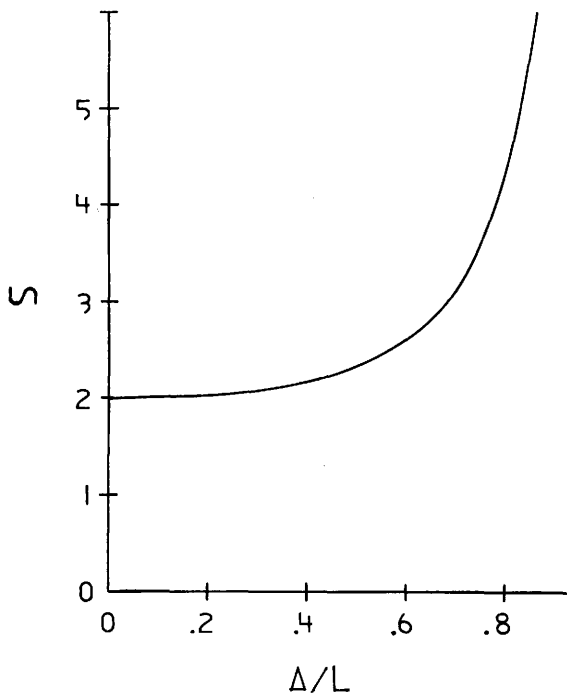
Figure 6. (S) vs. (Δ/L)
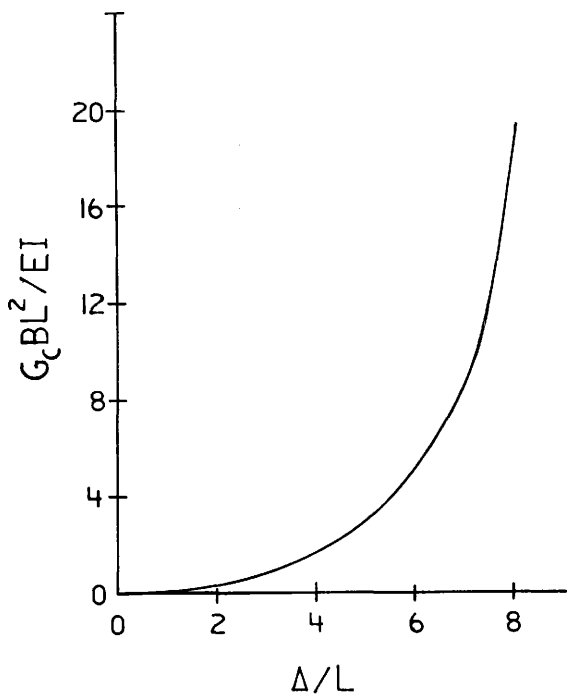
Figure 7. ($G_cBL^2/EI$) vs. ($\Delta/L$)

## EXPERIMENTAL PROCEDURE

In order to determine the critical energy release rate for a given material using the analytical technique previously developed in this thesis, an experimental procedure must be developed to be consistent with the assumptions utilized in the analytic formulation. This section will present the specimen fabrication and specimen test procedures which conforms to these assumptions.

### Specimen Preparation

All test specimens were made from 3M Scotchply Reinforced Plastic Type 1003. Type 1003 is an uncured prepreg tape containing a continuous "E" type fiberglass filament. The material was kept in a storage freezer at -18°C to enhance and prolong the shelf-life. Prior to use, the material was allowed to thaw at room temperature in its protective plastic bag for twenty-four hours to prevent moisture condensation on the material.

The prepreg tape was cut into 12" x 12" unidirectional sheets. Three different thickness panels were laid up for final cure. The layup, cure, and post-cure cycles for each of the 8, 12, and 16 ply panels were carefully repeated to create similiar material properties in each panel.

The layup and subsequent cure and post-cure cycles used for the laminate fabrication are detailed in Appendix D. After completion of these cycles the final test specimens were cut into approximately one inch wide unidirectional test strips. These specimens are shown in Figure 8.
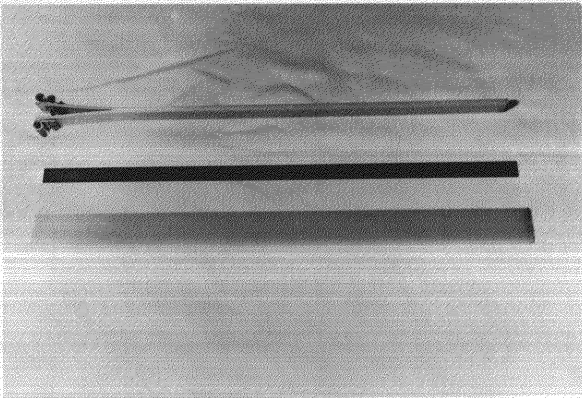
Figure 8. Test specimen configuration.

## Test Procedure

Each specimen was installed in an Instron test machine using a specially designed set of test grips. These grips were designed in a manner that enabled the load to be applied along a fixed line of action while permitting a virtually free rotation of the loaded ends of the double cantilever beam. This fixture best represented the conditions depicted previously in Figure 3. The local end moment, due to the load application point being different from the neutral axis location of the beam, is negligible. Therefore, the effects of thickness will be neglected.

A one thousand pound load cell was used in the Instron. This load cell was calibrated using the internal calibration resistors in the Instron. After proper calibration, a full scale displacement which corresponds to a load of twenty pounds was used when monitoring the applied load during the test. Prior to the installation of the specimen in the lower grip, the weight of the specimen and the upper grip were accounted for by zeroing the recorder pen. The crosshead displacement was set at a constant rate of one inch per minute. During the test the horizontal axis of the strip chart recorder was driven by the output of the load cell, while the vertical axis was driven by a time base function which had a direct one to one correspondence with the crosshead displacement.

Once installed in the test machine, the specimen is in a pre-test equilibrium position. An initial displacement existed in this position due to the grip placement and geometry and must be accounted for in the data reduction. This can be seen in the photographs in Figure 9,
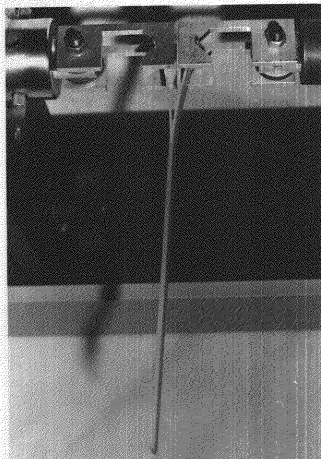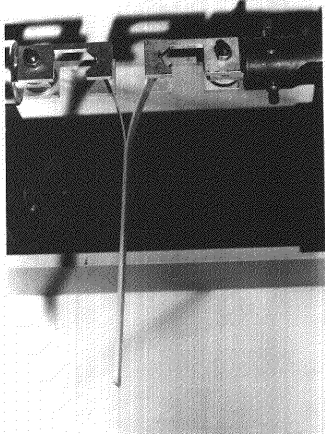
Figure 9. Double cantilever beam test sequence.
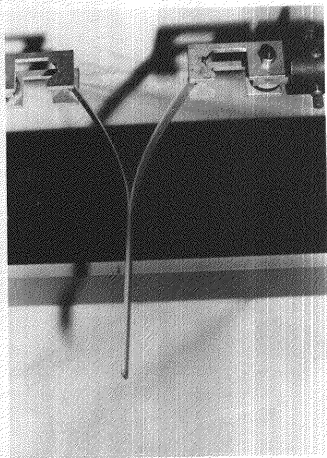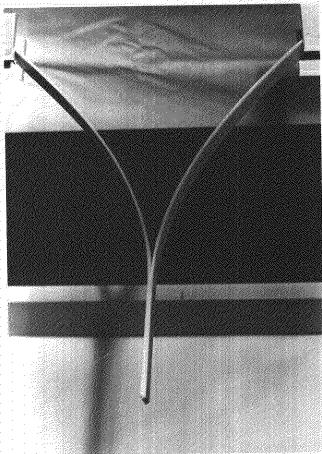
Figure 9. (continued)

which depict an actual test sequence. Observation of the load-dis-
placement recording showed that during the test the load initially
increased to a threshold value before dropping off as crack propaga-
tion began.

The sequence of events in a test in which both load and dis-
placement are continuously changing is depicted schematically in Figure
10. This figure coupled with the following explanation shows how the
requirement of constant displacement during crack propagation in
Equation (11) is satisfied. The dotted line represents the actual ex-
perimental data derivable from this type of a test. Figure 10 shows a
hypothetical path between points (a) and (e). The assumptions here are
that as one traverses from point (a) to point (b) there is no crack
extension premitted, but only a change in the stored strain energy
system. Once at point (b) the grip displacement is held constant while
the strain energy is allowed to dissipate in the form of crack ex-
tension. When the energy release rate ($\delta W/\delta L$) is no longer greater
than the critical value for crack extension ($G_c$) one arrives at point
(c) and the cycle repeats itself. This corresponds with the calculation
of the critical energy release rate at a constant grip displacement as
seen in Equation (11) on a piecewise basis. For the case of continuous
loading the requirements of Equation (11) are approximated if the rate
dependence of the material is negligible.

Due to the partial transparency of scotchply a light was positioned
over the top of the specimen, so that a shadow from the crack front
could be optically monitored during the test. The photograph in Figure
11 shows the visual characteristics of this crack front in a loaded
specimen. Throughout the test the crack front was monitored and as it
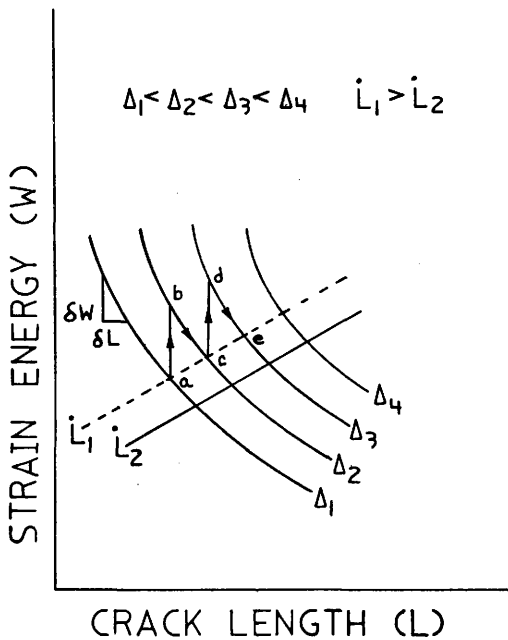
Figure 10. Theoretical crack extension theory
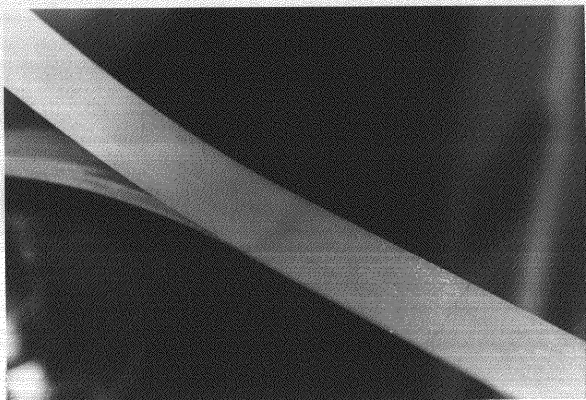
Figure 11. An illuminated test specimen highlighting the crack front.

passed the prescribed beam lengths, a reference mark was made on the load-displacement curve being recorded.  These marks allow the test data to be recorded as a function of the effective beam length.

In the next section, one set of experimental data is reduced in order to demonstrate how the critical energy release rate and critical stress intensity factor are determined from measured results.

EXPERIMENTAL RESULTS

The test specimens were subjected to a continuously changing
load and displacement during the actual test. The strip chart data
from the Instron contained all of the appropriate test parameters
needed for data reduction. Both load and displacement were monitored
as functions of the effective beam length and this data is tabulated
in Appendix F. Table 1 shows an example of the data extracted from
the strip chart recorder during the test. This data will be utilized
in the following section on data reduction, where some sample calcu-
lations will be carried out. This is done to aid the reader in
understanding the assumptions used in the subsequent data reduction.

## Sample Calculations for Data Reduction

The first step in reducing the data is to determine the values
of $\Delta/L$ for the test, in that, all parameters from the analysis were
presented graphically as functions of $\Delta/L$. It is important, however,
to retain the relationship between $\Delta/L$ and the initial effective
beam length (L). After determining $\Delta/L$, graphical interpolation
can be done to determine $(PL^2/EI)$, $(WL/EI)$, and (S). Lagrangian
interpolation was used as the method for evaluating the intermediate
values of these functions given the test values of $\Delta/L$. The interpo-
lation results for the sample data are presented in Table 2.

Using the value determined for $(PL^2/EI)$ as a function of $\Delta/L$
and the corresponding measured value of the load (P) an effective
flexural rigidity (EI) can be calculated. Results for this calculation
are summarized in Table 3. All required parameters are now available

Table 1.  Sample Test Data Specimen 12-4

| Length (L - in.) | Load (P - lbs.) | Displacement (2Δ - in.) |
|---|---|---|
| 3.5 | 6.07 | 2.22 |
| 4.0 | 5.48 | 2.85 |
| 4.5 | 4.97 | 3.61 |
| 5.0 | 4.62 | 4.37 |
| 5.5 | 4.25 | 5.14 |
| 6.0 | 3.99 | 5.96 |
| 6.5 | 3.81 | 6.92 |
| 7.0 | 3.67 | 7.80 |
| 7.5 | 3.54 | 8.83 |
| 8.0 | 3.33 | 9.71 |
| 8.5 | 3.17 | 10.58 |
| 9.0 | 2.91 | 11.38 |
| 9.5 | 2.97 | 12.64 |
| 10.0 | 3.01 | 13.81 |

Table 2.  Interpolation Data Specimen 12-4

| L | $\Delta/L$ | $PL^2/EI$ | WL/EI | S |
|------|-------|--------|--------|--------|
| 3.5 | .3171 | 1.0681 | .1596 | 2.1238 |
| 4.0 | .3563 | 1.2307 | .2045 | 2.1560 |
| 4.5 | .4011 | 1.4446 | .2644 | 2.1919 |
| 5.0 | .4370 | 1.6420 | .3198 | 2.2338 |
| 5.5 | .4672 | 1.8270 | .3719 | 2.2824 |
| 6.0 | .4967 | 2.0259 | .4285 | 2.3410 |
| 6.5 | .5323 | 2.2965 | .5051 | 2.4231 |
| 7.0 | .5571 | 2.5116 | .5647 | 2.4866 |
| 7.5 | .5887 | 2.8296 | .6491 | 2.5761 |
| 8.0 | .6069 | 3.0414 | .7027 | 2.6342 |
| 8.5 | .6224 | 3.2418 | .7515 | 2.6892 |
| 9.0 | .6322 | 3.3794 | .7840 | 2.7272 |
| 9.5 | .6653 | 3.9188 | .9044 | 2.8809 |
| 10.0 | .6905 | 4.4269 | 1.0089 | 3.0321 |

to determine $G_c$ using Equation (13). The value of the moment of inertia (I) and the width (B) for the individual specimens can be found in the geometric data tables in Appendix E. The apparent modulus and the critical energy rate normalized to the modulus are summarized and presented in Table 3 also.

## Summary of Experimental Results

Five specimens of each thickness, 8, 12, and 16 ply, were tested with the data recorded as a function of the beam length. For the purpose of further analysis the data was reduced for each specimen as done for the sample data. After the individual geometric parameters were isolated and removed from the data in order to eliminate any geometric bias, the data was grouped according to thickness. For a given thickness, the five data points for each respective specimen beam length were averaged in an attempt to reduce the experimental variance between specimens.

The averaged values of $E$, $\frac{G_c}{E}$, and $G_c$ calculated from the experimental data are shown in Figures 12 - 14 while the averaged experimental data from which these results were calculated is tabulated in Appendix G.

Table 3.  Material Parameters Specimen 12-4

| L | EI | E | $\frac{G_c BL^2}{EI}$ | $\frac{G_c}{E}$ | $G_c$ |
|---|---|---|---|---|---|
| (in.) | (lbs. in.$^2$) | (x $10^6$psi) | | (x $10^{-6}$ in.) | (lbs./in.) |
| 3.5 | 69.6143 | 5.9234 | .9972 | .9538 | 5.6498 |
| 4.0 | 71.2455 | 6.0622 | 1.2910 | .9454 | 5.7312 |
| 4.5 | 69.6693 | 5.9280 | 1.6882 | .9768 | 5.7906 |
| 5.0 | 70.3398 | 5.9851 | 2.0682 | .9694 | 5.8014 |
| 5.5 | 70.3700 | 5.9877 | 2.4416 | .9458 | 5.6630 |
| 6.0 | 70.9013 | 6.0329 | 2.8630 | .9318 | 5.6218 |
| 6.5 | 70.0948 | 5.9642 | 3.4580 | .9590 | 5.7198 |
| 7.0 | 71.5989 | 6.0922 | 3.9376 | .9416 | 5.7362 |
| 7.5 | 70.3710 | 5.9878 | 4.6426 | .9672 | 5.7908 |
| 8.0 | 70.0734 | 5.9624 | 5.1074 | .9350 | 5.5754 |
| 8.5 | 70.6492 | 6.0114 | 5.5448 | .8992 | 5.4058 |
| 9.0 | 69.7484 | 5.9348 | 5.8442 | .8454 | 5.0174 |
| 9.5 | 68.3997 | 5.8200 | 7.0194 | .9114 | 5.3040 |
| 10.0 | 67.9930 | 5.7854 | 8.1360 | .9534 | 5.5154 |
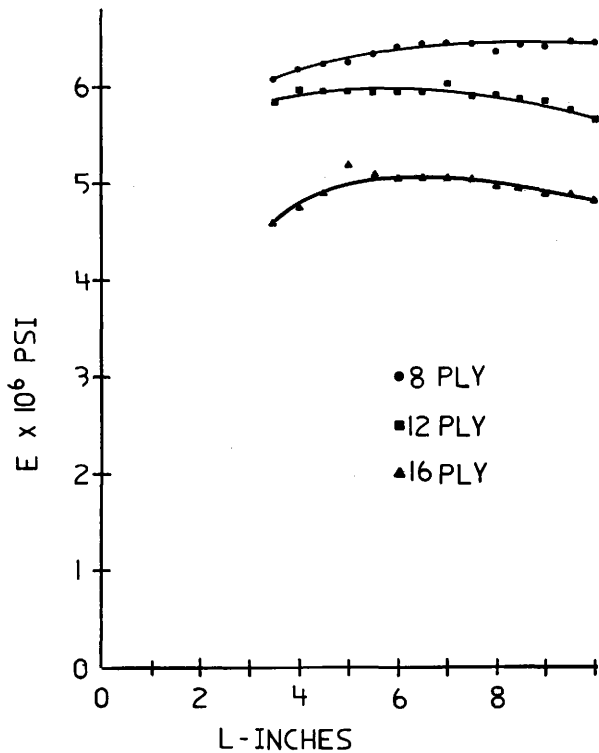
Figure 12. (E) vs. (L)
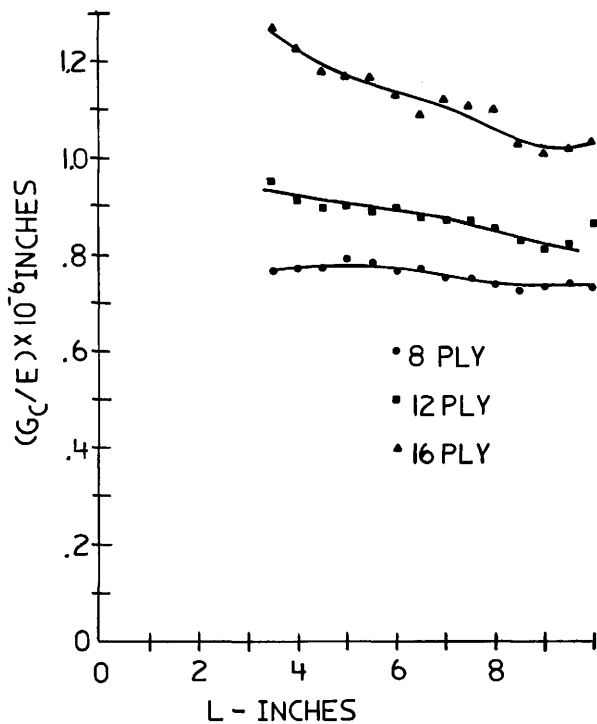
Figure 13 ($G_c/E$) vs. (L)
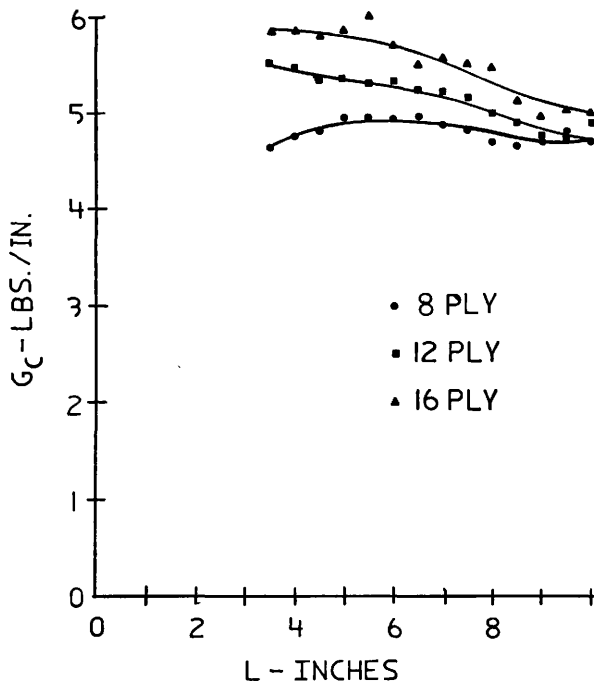
Figure 14. ($G_c$) vs. (L)

## DISCUSSION OF RESULTS

The relative magnitude of the effective modulus determined from the test data is seen to range between 4.5 and 6.5 x $10^6$ psi in Figure 12. These calculated values bracket the predicted manufacturer's value of 5.7 x $10^6$ psi. A variance from the predicted value is easily accounted for by means of the manufacturing process. Slight changes in the total resin content of the laminate during the cure cycle affect the overall modulus of the composite material.

A reasonable estimate for the critical energy release rate, $G_c$, is 5 lbs./in. As determined from Figure 14 where the three curves for $G_c$ vs. L for the various laminate thicknesses appear to converge. Utilizing the manufacturer's predicted value of $E_{22}$ of 1.4 x $10^6$ psi and Equation (2) a calculated value 1.87 ksi$\sqrt{in}$ for $K_{IC}$ is determined. Toughness values determined for scotchply in this investigation are compared to typical toughness values for other materials in Table 4.

The toughness values measured in this study are similar to those of other polymeric materials and are much lower than metals, as expected.

Implicit in the analysis is the assumption that, E, $G_c$, and $K_{IC}$ are material constants. Yet, an apparent variation in these quantities with crack length and laminate thickness are seen in Figures 12 - 14. These variations are apparent rather than real and reflect certain inadequancies in the analysis and the experiments. The causes of these apparent variations will be examined in the remainder of this section.

Table 4.  Typical Fracture Toughness Parameters ($K_{IC}$ and $G_c$)

| Material | $K_{IC}$ (ksi$\sqrt{in}$) | $G_c$ (lbs/in) |
|---|---|---|
| Metals [5, 10] | | |
| Ti-6Al-4V | 105 | 689 |
| 7075-T651 | 22 | 47 |
| 4340 | 55 – 90 | 104 – 279 |
| 2024 T3 | 40 | 152 |
| Thermoplastic Materials [11, 12] | | |
| Polymethyl Methacrylate | 1.46 – 1.74 | 6.05 |
| Polystyrene | .894 – 1.00 | 2.0 |
| Polyvinyl Chloride | 1.45 – 2.05 | 7.024 |
| Nylon – 6, 6 | .462 – .756 | 1.428 |
| Polyethylene | .756 – 1.069 | 28.5 |

Analytical Reasons for the Apparent Variations in $G_c$ and E

## Fiber Breakage

A close investigation of the photographs in Figure 9 reveal the presence of frayed and broken fibers in the area between the cantilever beam sections. The resulting degradation of fibers causes a discontinuity in the load path; thus, causing a reduction in the effective flexural rigidity of the beam. The resulting fiber breakage causes an increase in the energy release rate due to the actual fracture of these fibers. Observation of the three different test specimens under load revealed that the thinner the specimen the larger the deflections and the rotations. These larger deflections and rotations induce higher bending stresses in the outermost fibers, which would cause them to fail first, thus reducing the modulus.

Fiber breakage is considered to be a negligible effect in this investigation. This conclusion is based on the fact that the fiber breakage would be greatest in the 8 ply laminate, which would suggest a lower E and a higher measured $G_c$ for this material. This is just the reverse of the trends found experimentally, as seen in Figures 12 and 14. Furthermore, the maximum fiber stresses are less than the ultimate tensil strength of the material.

## Shear Effects Due to End Constraints

In the analytical formulation, the concept of a cantilever beam was used. The end conditions in a cantilever beam assumed that the boundary is rigid and the slope of the beam at the boundary goes to

zero.

In utilizing the double cantilever beam of this research effort a pseudo boundary is formed through the equilibrium state at the crack tip imposed by the opposing forces and moments in the respective beam sections.

These effects at the boundary can only be quantified with a finite element analysis. Qualitatively, the possibility of rotation at the boundary would cause the measured moduli to be an underestimate of the actual value. It is apparent from Figure 12 that this effect is minimal in that the experimental results for the 8 and 12 ply laminates are consistent with manufacturer's supplied data for the modulus.

Experimental Reasons for the Apparent Variation in $G_c$ and E

Processing Variations

As noted previously a change in the resin content will alter the material composition; thus, altering the effective modulus. Since all of the laminates were fabricated to the same manufacturing process, the only inconsistent variable remaining is the laminate thickness. In the formulation of a laminate the modulus is directly affected by the amount of resin flow and subsequent resin content, which is a direct function of the laminate thickness. For the thicker laminates a higher resin volume fraction results from the excess resin, which in turn leads to a lower value of modulus. This is consistent with the data trend in Figure 12, as there exists distinct banded regions for the values of E for the different thicknesses. The variation is seen

to increase as the laminates become thinner, which would be expected since the thinner laminates have a lower volume fraction.

## Strain Rate Sensitivity

In the description of the test method for Figure 11 a continuous test required that the strain rate sensitivity of the material be negligible. However, it was observed during the experimental phase that if the crosshead displacement was momentarily stopped, the resulting load decreased with time and the crack front continued to propagate until reaching the equilibrium conditon. Thus, the measured values for $G_c$ reflect a rate sensitivity, as shown in Figure 11. The variation in $G_c$ measured for various thicknesses and at various lengths may be fully explained by this dependence of $G_c$ on the crack growth rate.

Since this test was run at a constant crosshead displacement and the Λ/L variation for each specimen increased throughout the test, the value of the velocity of the crack front ($\dot{L}$) is decreasing through the test. The measured crack velocities for the various laminate thicknesses and crack lengths are summarized in Table 5.

The observed variation is $G_c$ with crack length (L) and laminate thickness (t) in Figure 14 correlates well with the variation in crack velocity ($\dot{L}$) for "L" and "t" summarized in Table 5. Qualitative agreement may be easily demonstrated if $G_c$ is proportional to $(\dot{L})^{0.2}$. This implies (L) is proportional to $(K_I^{10.0})$, which is reasonable in light of recent results on crack velocity in composite materials [13].

Table 5.  Strain Rate Variation (in./min.)

| No. of Laminate Plies | Beam Length Segments (in.) | 4.0 - 5.0 | 7.0 - 8.0 | 9.0 - 10.0 |
|---|---|---|---|---|
| 8 | | .50 | .50 | .50 |
| 12 | | .68 | .55 | .50 |
| 16 | | .85 | .57 | .50 |

## SUMMARY

This research effort developed a method for determining the delamination fracture toughness in the crack opening made for a unidirectional composite. Determination of the critical stress intensity factor $(K_{IC})$ is found independently of the other fracture modes. This allows for a check on other analytical techniques, which arrive at fracture toughness values through systems containing the presence of more than one fracture mode.

However, the apparent variations in material properties from this test must be minimized to reflect the actual material properties before utilizing the described technique to its fullest potential. Further investigation into the strain rate effects, previously described, will result in not only a means to minimize the apparent variation in $G_c$ but a better understanding into the viscoelastic effects of composite materials.

REFERENCES

1. 1974 Annual Book of ASTM Standards, E399-74, p. 432.

2. S. S. Wang, "Delamination Crack Growth in Unidirectional Fiber-Reinforced Composites Under Static and Cyclic Loading," ASTM Symposium on Composite Materials: Testing and Design (5th Conference), March 20, 1978, New Orleans, Louisiana.

3. S. S. Wang and J. F. Mandell, "Analysis of Delamination in Unidirectional and Crossplied Fiber-Composites Containing Surface Cracks," NASA Technical Report NASA-CR-135248, May, 1977.

4. J. F. Mandell, "Fatigue Crack Growth in Fiber Reinforced Plastics," 34th Annual Conference SPI Reinforced Plastic/Composites Institute, January, 1979, New Orleans, Louisiana.

5. R. W. Hertzberg, Deformation and Fracture Mechanics of Engineering Materials, Wiley, New York, 1976.

6. H. Tada, P. Paris, and G. Irwin, The Stress Analysis of Cracks Handbook, Del Research Corporation, 1973, p. 293.

7. G. S. Brockway and R. A. Schapery, "Some Viscoelastic Crack Growth Relations for Orthotropic Prestrained Media," Engineering Fracture Mechanics, 1978, Vol. 10, pp. 453, Pergamon Press.

8. K. E. Bisshopp and D. C. Drucker, "Large Deflection of Cantilever Beams," Quarterly of Applied Math, Vol. III, 1945, p. 272.

9. Samuel M. Selby (editor in chief), Standard Mathematical Tables, 19th Edition, The Chemical Rubber Co., Cleveland, Ohio, July, 1971.

10. Structural Design Data, Vought Aeronautics Division, LTV Aerospace Corporation, November, 1967.

11. E. Plati and S. G. Williams, "Effect of Temperature On the Impact Fracture Toughness of Polymers. Polymer, Vol. 16, December, 1975, p. 915.

12. M. M. Eisenstadt, Introduction to Mechanical Properties of Materials, Macmillan Company, N.Y., N.Y., 1971.

REFERENCES (continued)

13. J. C. Halpin, K. L. Jerina, and T. A. Johnson, "Characterization of Composites for the Purpose of Reliability Evaluation," _Analysis of the Test Methods for High Modulus Fibers and Composites_, pg. 5 ASTM, STP 521, 1973.

APPENDICES

APPENDIX A

Table A. 1.  Elliptic Integral Values

| | | | Elliptic Integrals | | | |
|---|---|---|---|---|---|---|
| | | | First Kind | | Second Kind | |
| | | | Comp | Incomp | Comp | Incomp |
| θ | k | φ | F(k, π/2) | F(k,φ) | E(k,π/2) | E(k, φ) |
| 45 | .7071 | 90.00 | 1.8541 | 1.8541 | 1.3506 | 1.3506 |
| 50 | .7660 | 67.38 | 1.9356 | 1.3414 | 1.3055 | 1.0429 |
| 55 | .8192 | 59.68 | 2.0347 | 1.1800 | 1.2587 | .9297 |
| 60 | .8660 | 54.74 | 2.1565 | 1.0783 | 1.2111 | .8555 |
| 65 | .9063 | 51.28 | 2.3088 | 1.0079 | 1.1638 | .8031 |
| 70 | .9397 | 48.81 | 2.5046 | .9579 | 1.1184 | .7655 |
| 75 | .9659 | 47.06 | 2.7681 | .9227 | 1.0764 | .7387 |
| 80 | .9848 | 45.89 | 3.1534 | .8992 | 1.0401 | .7207 |
| 85 | .9962 | 45.22 | 3.8317 | .8858 | 1.0127 | .7105 |
| 88 | .9994 | 45.03 | 4.7427 | .8821 | 1.0026 | .7076 |
| 90 | 1.0000 | 45.00 | ∞ | .8814 | 1.0000 | .7071 |

APPENDIX B

Table B.1.  Nonlinear Variables

| θ | k | α | $\frac{PL^2}{EI}$ | $\frac{\Delta}{L}$ | $\frac{WL}{EI}$ |
|---|---|---|---|---|---|
| 45 | .7071 | 0 | 0 | 0 | 0 |
| 50 | .7660 | .5942 | .3530 | .1161 | .0203 |
| 55 | .8192 | .8547 | .7305 | .2301 | .0819 |
| 60 | .8660 | 1.0782 | 1.1625 | .3404 | .1855 |
| 65 | .9063 | 1.3009 | 1.6923 | .4455 | .3339 |
| 70 | .9397 | 1.5467 | 2.3922 | .5437 | .5318 |
| 75 | .9659 | 1.8454 | 3.4057 | .6340 | .7901 |
| 80 | .9848 | 2.2542 | 5.0813 | .7167 | 1.1326 |
| 85 | .9962 | 2.9459 | 8.6780 | .7948 | 1.6488 |
| 88 | .9994 | 3.8606 | 14.9040 | .8472 | 2.2416 |
| 90 | 1.0000 | ∞ | ∞ | 1.0000 | ∞ |

## APPENDIX C

Strain energy derivation non-linear elastic beam

$$W = \frac{1}{2} \int_0^L \frac{M^2 ds}{EI}$$

$$M = EI \frac{d\phi}{ds} \qquad\qquad M^2 = (EI)^2 \left(\frac{d\phi}{ds}\right)^2$$

$$W = \frac{1}{2} \int_0^L EI \left(\frac{d\phi}{ds}\right)^2 ds$$

$$\left(\frac{d\phi}{ds}\right) = \left(\frac{2P}{EI}\right)^{1/2} (\sin \phi_0 - \sin \phi)^{1/2}$$

$$\left(\frac{d\phi}{ds}\right)^2 = \frac{2P}{EI} (\sin \phi_0 - \sin \phi)$$

$$W = \frac{1}{2} \int_0^L 2P (\sin \phi_0 - \sin \phi) ds$$

$$W = \int_0^{\phi_0} P(\sin \phi_0 - \sin \phi) \frac{ds}{d\phi} d\phi$$

$$\left(\frac{ds}{d\phi}\right) = \left(\frac{EI}{2P}\right)^{1/2} (\sin \phi_0 - \sin \phi)^{-1/2}$$

$$W = \int_0^{\phi_0} P \left(\frac{EI}{2P}\right)^{1/2} (\sin \phi_0 - \sin \phi)^{1/2} d\phi$$

$$W = \left(\frac{EIP}{2}\right)^{1/2} \int_{0}^{\phi_0} (\sin \phi_0 - \sin \phi)^{1/2} \, d\phi$$

$$\sin \phi = 2k^2 \sin^2 \theta - 1$$

$$\sin \phi_0 = 2k^2 - 1$$

$$\cos \phi \, \frac{d\phi}{d\theta} = 4k^2 \sin \theta \, \cos \theta$$

$$\frac{d\phi}{d\theta} = \frac{4k^2 \sin\theta \, \cos \theta}{\cos \phi}$$

$$\sin^2\phi = (2k^2 \sin^2 \theta - 1)^2 = 1 - \cos^2\phi$$

$$\cos^2\phi = 1 - (2k^2 \sin^2\theta - 1)^2$$

$$\cos \phi = 2k \sin \theta (1 - k^2 \sin^2\theta)^{1/2}$$

$$W = \left(\frac{EIP}{2}\right)^{1/2} \int_{\theta_1}^{\pi/2} \left(\left((2k^2 - 1) - (2k^2 \sin \theta - 1)\right)^{1/2}\right.$$

$$\left(\frac{4k^2 \sin \theta \, \cos \theta}{2 k \sin\theta(1 - k^2 \sin^2\theta)^{1/2}}\right)\right) d\theta$$

$$W = 2(EIP)^{1/2} \int_{\theta_1}^{\pi/2} \frac{k^2 \cos^2\theta}{(1 - k^2 \sin^2\theta)^{1/2}} \, d\theta$$

$$W = 2(EIP)^{1/2} \int_{\theta_1}^{\pi/2} \frac{k^2(1 - \sin^2\theta)}{(1 - k^2\sin^2\theta)^{1/2}} \ d\theta$$

$$W = 2(EIP)^{1/2} \int_{\theta_1}^{\pi/2} \frac{k^2 - k^2\sin^2\theta + 1 - 1}{(1 - k^2\sin^2\theta)^{1/2}} \ d\theta$$

$$W = 2(EIP)^{1/2} \left\{ \int_{\theta_1}^{\pi/2} \frac{k^2 - 1}{(1 - k^2\sin^2\theta)^{1/2}} \ d\theta \right.$$

$$\left. + \int_{\theta_1}^{\pi/2} (1 - k^2\sin^2\theta)^{1/2} \ d\theta \right\}$$

$$W = 2(EIP)^{1/2} \left\{ (k^2 - 1)(F(k, \pi/2) - F(k,\phi)) + (E(k, \pi/2) - E(k,\phi)) \right\}$$

$$\frac{WL}{EI} = 2\left(\frac{PL^2}{EI}\right)^{1/2} \left\{ (k^2 - 1)(F(k) - F(k, \phi) + E(k) - E(k, \phi)) \right\}$$

$$\frac{WL}{EI} = 2\alpha \left\{ (k - 1)\alpha + E(k) - E(k, \phi) \right\}$$

$$\frac{WL}{EI} = \alpha^2 \left\{ 2k - 2 + \frac{2(E(k) - E(k, \phi))}{\alpha} \right\}$$

$$\frac{WL}{EI} = \alpha^2 \left\{ -\frac{\Delta}{L} + 2k^2 - 1 \right\}$$

APPENDIX D

The layup procedure that was used to fabricate the test laminates is as
follows:

* The teflon coated base plate used in the laminate press was
  cleaned with acetone to remove any existing contaminates.

* In order to contain any excess resin flow during the cure cycle
  and to mold the laminates into square panels a picture frame of
  cork was attached to the base plate.

* Half of the desired plies were laid up in a unidirectional manner
  inside the picture frame.

* After half of the desired number of plies had been laid up, a
  two inch wide sheet of teflon film was placed normal to the fiber
  direction at one end of the laminate.  This was done to arti-
  ficially produce the desired crack front.

* The remaining plies were then placed in the picture frame to
  complete the unidirectional laminate.

* One sheet of teflon glass fabric was added to the top of the
  laminate to insure an easy release between the laminate and the
  bleeder cloth after the cure cycle.

* Next appropriate layers of number 120 bleeder cloth were placed
  in the picture frame.  The bleeder cloth was used to transport
  excess resin and volitales away from the laminate during the
  cure cycle.  The number of layers of bleeder cloth was deter-
  mined using the 3M recommendation of one layer of 120 for every
  three plies of prepreg tape.

* A 12" x 12" x .090" aluminum plate which had been previously

coated with Freekote 33 release agent was installed on top of
the bleeder cloth to equalize the pressure distribution on the
laminate during the cure cycle.

* The entire layup and cork picture frame were covered with a tef-
  lon sheet and bagged to the base plate.  The bagging process
  restrains the resin flow to a local area and reduces the pos-
  sibility of damage to the laminate press.

* The teflon bag was ventilated along the top to produce a vacuum
  path, with the aid of additional bleeder cloth, between the
  laminate and the vacuum ports in the base plate.

An exploded cross-sectional view of the entire bagged laminate as it is
seen prior to going through the cure cycle is illustrated in Figure D. 1.
The required cure cycle is as follows:

* The laminate press in the McNew Engineering Laboratory was pre-
  heated to a temperature of 300°F.

* After the press reached the desired temperature the base plate
  with the bagged laminate assembly on it was aligned in the press,
  with the vacuum ports in the base plate directly over the cor-
  responding vacuum ports in the bottom plate of the press.

* A rubber bladder was then rolled over the positioned base plate
  to seal the upper and lower cavities of the press from each
  other.

* Exposure to the preheated press begins to heat the laminate, so
  the cure cycle was considered to begin when the press was closed.

* After closing the press the lower portion of the press was
  pressurized to 90 psi to form a seal with the rubber bladder and
  the upper palate of the press.

1. Vacuum ports
2. Base plate
3. Cork damn
4. Prepreg tape
5. Teflon sheet
6. Teflon bleeder cloth
7. 120 bleeder cloth
8. Aluminum pressure plate
9. Teflon bag
10. Vacuum transport
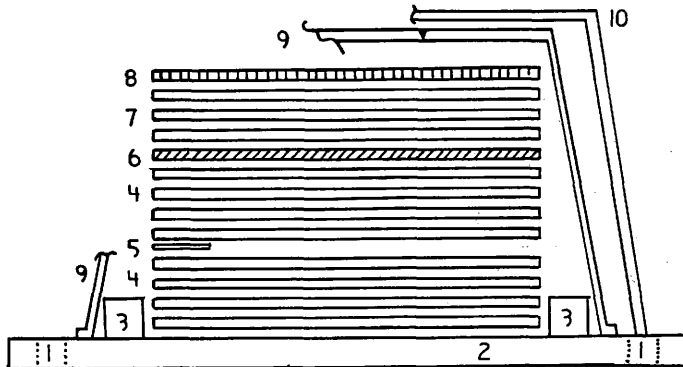


Figure D.1. Crossectional of a test laminate layup

* While the lower portion of the press was being pressurized, a vacuum was being drawn on the bagged assembly. An environmental note: the vacuum drawn on the system was routed through a liquid nitrogen trap to condense harmful volitales.

* After four minutes into the cure cycle the upper cavity was pressurized to 90 psi. No problem was caused by this reverse pressure on the previously established seal as the upper pressurized area was sufficiently less than that of the lower plate.

* After an additional five minutes (a total of nine) into the cure cycle, the temperature was raised to 330°F.

* After a total cure time of forty minutes the vacuum pump and the temperature controls were turned off.

* A uniform cool down rate under pressure is desired to minimize the effects of thermal gradients in the laminate. Currently, however, this is quite difficult to achieve with the manual flow controls on the coolant water supply valves. The rate of cool down was neglected in order to cool the upper and lower surfaces simultaneously within five degrees of each other.

* After achieving room temperature the cured laminates were removed from the base plate and placed in a post-cure oven at 300°F for twelve hours.

* At completion of the twelve hour post-cure the oven was turned off. The specimens remained in the oven and were allowed to cool slowly back to room temperature before further preparation.

* The final test specimens were cut into approximately one inch wide unidirectional strips. These specimens are shown in the photograph in Figure 9.

APPENDIX E

Table E.1. Geometric Data 8 Ply

|  | 8-1 | 8-2 | 8-3 | 8-4 | 8-5 |
|---|---|---|---|---|---|
| Thickness (in.) | .0653 | .0662 | .0669 | .0671 | .0673 |
| Width (in.) | .9933 | 1.0029 | 1.0037 | 1.0028 | 1.0029 |
| I ($*10^{-6}$ in.$^4$) | 2.8810 | 3.0308 | 3.1305 | 3.1558 | 3.1844 |

Table E.2. Geometric Data 12 Ply

|  | 12-1 | 12-2 | 12-3 | 12-4 | 12-5 |
|---|---|---|---|---|---|
| Thickness (in.) | .0978 | .1033 | .1037 | .1040 | .1033 |
| Width (in.) | 1.0023 | 1.0026 | 1.0028 | 1.0030 | 1.0025 |
| I ($*10^{-6}$ in.$^4$) | 9.7666 | 11.5122 | 11.6488 | 11.7525 | 11.5110 |

Table E.3.  Geometric Data 16 Ply

|                          | 16-1    | 16-2    | 16-3    | 16-4    | 16-5    |
|--------------------------|---------|---------|---------|---------|---------|
| Thickness (in.)          | .1279   | .1333   | .1348   | .1350   | .1345   |
| Width (in.)              | .9914   | 1.0022  | 1.0027  | .9032   | 1.0035  |
| I ($*10^{-6}$ in.$^4$)   | 21.6067 | 24.7271 | 25.5841 | 23.1480 | 25.4339 |

APPENDIX F

Table F.1. Displacement (2Δ) 8 Ply

| L | 8-1 | 8-2 | 8-3 | 8-4 | 8-5 |
|------|-------|-------|-------|-------|-------|
| 3.5 | 3.60 | 3.49 | 3.64 | 3.48 | 3.39 |
| 4.0 | 4.58 | 4.525 | 4.525 | 4.45 | 4.34 |
| 4.5 | 5.60 | 5.44 | 5.50 | 5.48 | 5.23 |
| 5.0 | 6.62 | 6.49 | 6.52 | 6.54 | 6.33 |
| 5.5 | 7.63 | 7.50 | 7.56 | 7.46 | 7.30 |
| 6.0 | 8.66 | 8.46 | 8.50 | 8.46 | 8.29 |
| 6.5 | 9.64 | 9.53 | 9.52 | 9.39 | 9.51 |
| 7.0 | 10.54 | 10.51 | 10.50 | 10.43 | 10.55 |
| 7.5 | 11.60 | 11.43 | 11.56 | 11.44 | 11.54 |
| 8.0 | 12.64 | 12.48 | 12.50 | 12.44 | 12.47 |
| 8.5 | 13.63 | 13.50 | 13.56 | 13.42 | 13.35 |
| 9.0 | 14.73 | 14.59 | 14.54 | 14.39 | 14.39 |
| 9.5 | 15.76 | 15.70 | 15.59 | 15.36 | 15.36 |
| 10.0 | 16.78 | 16.62 | 16.60 | 16.42 | 16.30 |

Table F.2. Load (P) 8 Ply

| L | 8-1 | 8-2 | 8-3 | 8-4 | 8-5 |
|------|------|------|------|------|------|
| 3.5 | 3.12 | 3.24 | 3.32 | 3.32 | 3.10 |
| 4.0 | 2.84 | 3.10 | 3.10 | 3.16 | 2.92 |
| 4.5 | 2.74 | 2.98 | 2.92 | 3.02 | 2.68 |
| 5.0 | 2.76 | 2.88 | 2.75 | 3.06 | 2.60 |
| 5.5 | 2.62 | 2.78 | 2.70 | 2.85 | 2.64 |
| 6.0 | 2.60 | 2.66 | 2.62 | 2.72 | 2.54 |
| 6.5 | 2.56 | 2.60 | 2.54 | 2.56 | 2.76 |
| 7.0 | 2.40 | 2.60 | 2.46 | 2.54 | 2.60 |
| 7.5 | 2.34 | 2.42 | 2.44 | 2.48 | 2.64 |
| 8.0 | 2.30 | 2.38 | 2.36 | 2.42 | 2.42 |
| 8.5 | 2.27 | 2.40 | 2.40 | 2.40 | 2.30 |
| 9.0 | 2.36 | 2.56 | 2.37 | 2.28 | 2.26 |
| 9.5 | 2.50 | 2.70 | 2.35 | 2.20 | 2.18 |
| 10.0 | 2.58 | 2.50 | 2.30 | 2.26 | 2.06 |

Table F.3.  Displacement (2Δ) 12 Ply

| L | 12-1 | 12-2 | 12-3 | 12-4 | 12-5 |
|---|------|------|------|------|------|
| 3.5 | 2.31 | 2.22 | 2.30 | 2.22 | 2.25 |
| 4.0 | 2.93 | 2.80 | 2.87 | 2.85 | 2.89 |
| 4.5 | 3.60 | 3.48 | 3.58 | 3.61 | 3.47 |
| 5.0 | 4.36 | 4.30 | 4.34 | 4.37 | 4.21 |
| 5.5 | 5.14 | 5.14 | 5.09 | 5.14 | 5.01 |
| 6.0 | 6.02 | 6.01 | 6.02 | 5.96 | 5.84 |
| 6.5 | 6.85 | 6.89 | 6.81 | 6.92 | 6.57 |
| 7.0 | 7.70 | 7.81 | 7.69 | 7.80 | 7.58 |
| 7.5 | 8.59 | 8.84 | 8.73 | 8.83 | 8.21 |
| 8.0 | 9.52 | 9.64 | 9.70 | 9.71 | 9.10 |
| 8.5 | 10.62 | 10.66 | 10.55 | 10.58 | 9.96 |
| 9.0 | 11.48 | 11.61 | 11.45 | 11.38 | 10.95 |
| 9.5 | 12.65 | 12.52 | 12.30 | 12.64 | 12.00 |
| 10.0 | 13.87 | 13.65 | 13.45 | 13.81 | 13.30 |

Table F.4. Load (P) 12 Ply

| L | 12-1 | 12-2 | 12-3 | 12-4 | 12-5 |
|------|------|------|------|------|------|
| 3.5 | 5.41 | 5.61 | 5.93 | 6.07 | 6.17 |
| 4.0 | 4.85 | 5.01 | 5.39 | 5.48 | 5.32 |
| 4.5 | 4.35 | 4.39 | 4.89 | 4.97 | 4.71 |
| 5.0 | 3.95 | 4.19 | 4.55 | 4.62 | 4.27 |
| 5.5 | 3.65 | 3.95 | 4.19 | 4.25 | 3.92 |
| 6.0 | 3.42 | 3.82 | 4.00 | 3.99 | 3.67 |
| 6.5 | 3.19 | 3.59 | 3.71 | 3.81 | 3.35 |
| 7.0 | 3.01 | 3.45 | 3.51 | 3.67 | 3.27 |
| 7.5 | 2.82 | 3.33 | 3.45 | 3.54 | 3.89 |
| 8.0 | 2.72 | 3.07 | 3.29 | 3.33 | 2.71 |
| 8.5 | 2.67 | 2.99 | 3.11 | 3.17 | 2.53 |
| 9.0 | 2.57 | 2.89 | 2.93 | 2.91 | 2.47 |
| 9.5 | 2.57 | 2.75 | 2.72 | 2.97 | 2.39 |
| 10.0 | 2.57 | 2.73 | 2.62 | 3.01 | 2.44 |

Table F.5. Displacement (2Δ) 16 Ply

| L | 16-1 | 16-2 | 16-3 | 16-4 | 16-5 |
|------|-------|-------|-------|-------|-------|
| 3.5 | 1.80 | 1.88 | 1.78 | 1.80 | 1.78 |
| 4.0 | 2.31 | 2.40 | 2.27 | 2.29 | 2.20 |
| 4.5 | 2.83 | 2.89 | 2.86 | 2.90 | 2.64 |
| 5.0 | 3.50 | 3.60 | 3.34 | 3.50 | 3.26 |
| 5.5 | 4.17 | 4.30 | 4.00 | 4.17 | 3.97 |
| 6.0 | 4.85 | 4.90 | 4.71 | 4.77 | 4.62 |
| 6.5 | 5.61 | 5.49 | 5.30 | 5.46 | 5.40 |
| 7.0 | 6.40 | 6.34 | 6.09 | 6.31 | 6.20 |
| 7.5 | 7.07 | 7.14 | 7.05 | 7.15 | 7.00 |
| 8.0 | 7.87 | 7.80 | 7.85 | 8.16 | 7.74 |
| 8.5 | 8.55 | 8.40 | 8.57 | 8.91 | 8.67 |
| 9.0 | 9.33 | 9.14 | 9.51 | 9.83 | 9.40 |
| 9.5 | 10.33 | 10.04 | 10.63 | 10.75 | 10.32 |
| 10.0 | 11.40 | 10.96 | 11.60 | 11.69 | 11.29 |

Table F.6. Load (P) 16 Ply

| L | 16-1 | 16-2 | 16-3 | 16-4 | 16-5 |
|------|------|------|------|------|------|
| 3.5 | 6.85 | 8.16 | 7.44 | 7.65 | 7.94 |
| 4.0 | 6.15 | 7.14 | 6.79 | 6.95 | 7.04 |
| 4.5 | 5.45 | 6.49 | 6.16 | 6.45 | 6.14 |
| 5.0 | 5.11 | 6.08 | 5.49 | 5.90 | 5.72 |
| 5.5 | 4.73 | 5.71 | 5.24 | 5.49 | 5.49 |
| 6.0 | 4.37 | 5.14 | 4.74 | 4.82 | 5.02 |
| 6.5 | 4.25 | 4.54 | 4.24 | 4.57 | 4.74 |
| 7.0 | 3.85 | 4.39 | 4.08 | 4.35 | 4.54 |
| 7.5 | 3.46 | 4.14 | 3.96 | 4.19 | 4.30 |
| 8.0 | 3.24 | 3.74 | 3.67 | 4.05 | 4.00 |
| 8.5 | 2.98 | 3.36 | 3.44 | 3.75 | 3.84 |
| 9.0 | 2.83 | 3.14 | 3.34 | 3.47 | 3.54 |
| 9.5 | 2.75 | 2.99 | 3.29 | 3.44 | 3.44 |
| 10.0 | 2.65 | 2.87 | 3.14 | 3.29 | 3.34 |

APPENDIX G

Table G. 1.  Averaged Material Parameters–Modulus (E x $10^6$ psi)

| L | 8 Ply | 12 Ply | 16 Ply |
|---|---|---|---|
| 3.5 | 6.0848 | 5.8442 | 4.6009 |
| 4.0 | 6.1830 | 5.9886 | 4.7650 |
| 4.5 | 6.2372 | 5.9683 | 4.8989 |
| 5.0 | 6.2457 | 5.9670 | 5.1913 |
| 5.5 | 6.3374 | 5.9567 | 5.0930 |
| 6.0 | 6.4059 | 5.9646 | 5.0505 |
| 6.5 | 6.4426 | 5.9600 | 5.0531 |
| 7.0 | 6.4570 | 6.0015 | 5.0607 |
| 7.5 | 6.4388 | 5.9391 | 5.0581 |
| 8.0 | 6.3539 | 5.9044 | 4.9668 |
| 8.5 | 6.4334 | 5.8777 | 4.9531 |
| 9.0 | 6.4148 | 5.8784 | 4.9082 |
| 9.5 | 6.4767 | 5.7853 | 4.8986 |
| 10.0 | 6.4411 | 5.6577 | 4.8182 |

Table G. 2.  Averaged Material Parameter – ($G_c/E \times 10^{-6}$ in.)

| L | 8 Ply | 12 Ply | 16 Ply |
|------|-------|--------|--------|
| 3.5 | .7657 | .9481 | 1.2736 |
| 4.0 | .7697 | .9160 | 1.2279 |
| 4.5 | .7703 | .8977 | 1.1833 |
| 5.0 | .7921 | .8996 | 1.1746 |
| 5.5 | .7812 | .8887 | 1.1758 |
| 6.0 | .7655 | .8951 | 1.1294 |
| 6.5 | .7723 | .8774 | 1.0891 |
| 7.0 | .7572 | .8738 | 1.1009 |
| 7.5 | .7508 | .8694 | 1.0897 |
| 8.0 | .7384 | .8472 | 1.0802 |
| 8.5 | .7255 | .8340 | 1.0321 |
| 9.0 | .7330 | .8088 | 1.0109 |
| 9.5 | .7394 | .8182 | 1.0270 |
| 10.0 | .7308 | .8640 | 1.0367 |

Table G. 3. Averaged Material Parameter - Critical Energy Relaease
Rate ($G_c$ - 1bs./in.)

| L | 8 Ply | 12 Ply | 16 Ply |
|------|-------|--------|--------|
| 3.5 | 4.642 | 5.536 | 5.860 |
| 4.0 | 4.758 | 5.482 | 5.848 |
| 4.5 | 4.802 | 5.352 | 5.796 |
| 5.0 | 4.950 | 5.362 | 5.868 |
| 5.5 | 4.942 | 5.248 | 5.994 |
| 6.0 | 4.922 | 5.336 | 5.704 |
| 6.5 | 4.976 | 5.226 | 5.510 |
| 7.0 | 4.886 | 5.240 | 5.578 |
| 7.5 | 4.832 | 5.160 | 5.518 |
| 8.0 | 4.690 | 5.000 | 5.376 |
| 8.5 | 4.664 | 4.904 | 5.126 |
| 9.0 | 4.700 | 4.750 | 4.966 |
| 9.5 | 4.790 | 4.734 | 5.036 |
| 10.0 | 4.706 | 4.892 | 5.000 |

VITA

Daniel Frank Devitt was born September 23, 1953, in West Bend, Wisconsin, the son of Harry and Mary Devitt of Whitewater, Wisconsin. After graduating from Addison Trail High School, Addison, Illinois, in 1971, Daniel enrolled in the engineering school at Purdue University. Requirements for the degree of Bachelor of Science in Aeronautical and Astronautical Engineering were completed in May of 1975. Upon receipt of said degree, employment was secured at Vought Corporation of Dallas, Texas, where Daniel has been gainfully employed every since. Daniel is a member of the Structural Technologies Department at Vought where he is a Structural Engineer. Additional education includes successful completion of The Associate Engineer Development Program at Vought in December of 1975. Prior to enrolling in the Graduate School at Texas A&M, Daniel was enrolled at the University of Texas at Arlington in the Engineering Mechanics School.

Permanent Mailing Address:   3709 Greenhill Lane
Grand Prairie, Texas  75051